

# The Case for UHF-Band MU-MIMO

Narendra Anand, Ryan E. Guerra, and Edward W. Knightly  
Rice University, Houston, TX, USA  
{nanand,war,knightly}@rice.edu

## ABSTRACT

While the UHF band exhibits superior propagation characteristics compared to other frequency bands used for broadband communications, limited spectral availability in time and space necessitates high spectral efficiency techniques such as Multi-user MIMO (MU-MIMO). In this paper we design and implement the first open MU-MIMO Software-Defined Radio (SDR) platform that operates on an order of magnitude frequency range, from 300 MHz to 5.8 GHz. We perform a comprehensive set of over-the-air experiments to evaluate the potential of UHF-band MU-MIMO in comparison to 2.4 and 5.8 GHz WiFi bands encompassing a range of operating environments. We evaluate MU-MIMO performance in both outdoor, indoor, line-of-sight (LOS), and non-line-of-sight (NLOS) environments, and demonstrate that while the temporal correlation of the measured UHF environment is increased, it does not come at the cost of increased spatial correlation as measured by the Demmel condition number, thus proving highly attractive for MU-MIMO. This evaluation demonstrates the effectiveness of MU-MIMO transmission techniques in UHF bands for high spectral efficiency and low-overhead wireless access.

## Categories and Subject Descriptors

C.2.1 [Computer-Communication Networks]: Network Architecture and Design—*Wireless Communication*

## General Terms

Measurement, Performance, Reliability, Experimentation, Design

## Keywords

Multi-user MIMO, Beamforming, UHF, Channel State Information, Channel Measurement, Channel Correlation, Demmel Condition Number

Permission to make digital or hard copies of all or part of this work for personal or classroom use is granted without fee provided that copies are not made or distributed for profit or commercial advantage and that copies bear this notice and the full citation on the first page. Copyrights for components of this work owned by others than the author(s) must be honored. Abstracting with credit is permitted. To copy otherwise, or republish, to post on servers or to redistribute to lists, requires prior specific permission and/or a fee. Request permissions from [permissions@acm.org](mailto:permissions@acm.org).

*MobiCom'14*, September 7-11, 2014, Maui, Hawaii, USA.

Copyright is held by the owner/author(s). Publication rights licensed to ACM.

ACM 978-1-4503-2783-1/14/09 ...\$15.00.

<http://dx.doi.org/10.1145/2639108.2639144>.

## 1. INTRODUCTION

Multi-user MIMO (MU-MIMO) is a transmission technique that enables a multi-antenna transmitter to transmit multiple, parallel data streams to distinct user nodes. By pre-coding the data streams concurrently through a coherent antenna array, a transmitter can increase its spectral efficiency and overall downlink system capacity. Closed-loop MU-MIMO transmissions first require a transmitter to measure the channel between itself and its receivers (a process known as channel sounding) before transmitting concurrent data streams to the receivers. This direct measurement of Channel State Information (CSI) adds considerable protocol overhead and must occur more often in time-varying channel environments since the beam-formed transmission is sensitive to channel variation. A more temporally-correlated channel would allow a MU-MIMO system to reduce CSI-estimation frequency and improve the accuracy of this estimate for longer lag times.

State-of-the-art MU-MIMO channel models based on empirical measurements have been developed that predict increased channel correlation in lower frequency bands, but are inconclusive with respect to the effect on receiver separability simply because a direct comparison of diverse frequency bands in the same environment has not been attempted [27, 36]. For instance, one might assume that increased propagation through building materials might reduce the amount of multi-path for an indoor environment compared to an 802.11n WLAN [16]. This would have the effect of reducing the ability of a MU-MIMO base station to beam-form separate spatial streams to simultaneous users. Without a comparative study of different frequency bands, it is hard to draw conclusions for UHF



Figure 1: The WURC-enabled MU-MIMO array.

MU-MIMO performance from existing work in 802.11n WLANs [9].

While the recent switch to digital television has released hundreds of megahertz of spectrum in the VHF/UHF frequency band for reassignment (54 MHz to 698 MHz in the United States and 470 MHz to 790 MHz in Europe [8, 12]), only a limited number of channels are available in some locations and in many cases those channels are non-contiguous.

Although both 5 GHz and UHF bands have roughly 600 MHz of available spectrum, many sections of the sub-gigahertz range are already assigned to different licensed technologies (e.g., broadcast television, cellular networks). While the propagation characteristics of the UHF band are more desirable, limited spectrum availability at these frequencies necessitates high spectral efficiency in order to achieve high throughput performance. The expected increased channel temporal correlation may compensate for diminished spectrum in the UHF band by enabling robust, low-overhead MU-MIMO operation, so long as it does not come at the cost of increased spatial correlation between users' wireless channels.

In this paper, we evaluate the efficacy of UHF MU-MIMO in comparison to 2.4 and 5 GHz WiFi bands and make the case for its adoption in a wide variety of transmission scenarios. To accomplish this goal, we design and implement the first open MU-MIMO Software-Defined Radio (SDR) platform that operates on an order of magnitude frequency range, from 300 MHz to 5.8 GHz, shown in Fig. 1. As a key enabling technology, we design and implement WURC, a wideband, high-power SDR front-end for this Wireless Open-access Research Platform (WARP)-based MU-MIMO array (the red daughtercards shown in Fig. 1). WURC is a high-power RF front end that attaches to Xilinx and Altera-based SDR platforms which supplements WARP with a transmitter capable of operation from 300 MHz to 3.8 GHz and optimized for high transmit power for outdoor, long-range links.

We make the following contributions:

- We develop a UHF MU-MIMO testbed using the WARPv3 SDR combined with custom designed UHF daughtercards, allowing for MU-MIMO transmissions in spectrum with an order of magnitude difference (300 MHz to 5.8 GHz) and high UHF transmit power in a small form factor.
- We characterize the UHF MU-MIMO channel in various transmission environments and perform side-by-side comparisons using WARPLab with the 2.4 GHz and 5 GHz WiFi band to verify the theoretical characteristics of each.
- For longer-range topologies that are beyond the capabilities of WARPLab and for fine grain channel characterization, we implement a high speed channel sounding framework that allows for the collection of 4x transmit antenna, wideband channel matrices every 800  $\mu$ s to an arbitrary number of receivers.
- We find that while the UHF environment demonstrates a relatively similar degree of spatial correlation measured by channel condition number, when compared to other WLAN technologies, it demonstrates superior temporal correlation, thus proving attractive for MU-MIMO techniques.

In the rest of this paper, we first provide the necessary background for MU-MIMO transmissions in § 2; discuss the design, implementation, and verification of the open-source UHF MU-MIMO testbed in § 3; present a model-based analysis of indoor and outdoor MU-MIMO environments in § 4 which is compared to over-the-air experiments utilizing the developed MU-MIMO testbed in § 5; and present related work in § 6 with closing remarks in § 7.

## 2. BACKGROUND

In this section we briefly discuss MU-MIMO transmission techniques and how the inherent spectrum differences between UHF and 2.4/5 GHz frequency bands affect MU-MIMO transmission performance.

### 2.1 Multi-user Beamforming

Multi-user beamforming is a multi-antenna transmission technique that allows a transmitter to spatially reuse a wireless channel by transmitting multiple concurrent streams. This is achieved in two steps: First, each data stream is multiplied by a length  $M$  vector of complex steering weights (where  $M$  is the number of transmit antennas) resulting in  $M$  phase twisted copies of each data stream. Second, each receiver's set of  $M$  copies are summed together at each antenna to construct  $K$  parallel data streams (where  $K$  is the number of concurrent receivers) emanating from  $M$  antennas.

**Weight Selection.** Weights are chosen such that the interference between the parallel streams is minimal. To compute these weights, the transmitter must first measure the channel state matrix ( $H$ ) where each element corresponds to the magnitude and phase difference between each transmit and receive antenna. The optimal method of constructing the steering matrix is Dirty Paper Coding (DPC) [14]; however, its complexity makes it unfeasible to implement. Instead, a method known as Zero-forcing Beamforming (ZFBF) is shown to approach the optimal performance of DPC while employing a computationally feasible weight matrix calculation method, the pseudo-inverse [34] given by

$$W = H^\dagger = H^* \cdot (H \cdot H^*)^{-1}. \quad (1)$$

A key element of ZFBF is the zero-interference condition which is a direct result of the pseudo-inverse. Because  $W = H^\dagger$ ,  $h_i w_j = 0$  for  $i \neq j$  meaning that the interference from user  $i$ 's stream on user  $j$  is nulled and vice versa. ZFBF precodes the transmitted data streams such that the combined wireless channel between the transmitter and the receivers ( $H$ ) is separated. If ZFBF works perfectly, we can express the precoded transmission ( $W \cdot \text{Tx}$ ) as:

$$\begin{aligned} W \cdot \text{Tx} &\xrightarrow{H} H \cdot (W \cdot \text{Tx}) \\ &= I \cdot (\text{Tx}) = \text{Tx} \end{aligned} \quad (2)$$

In our work, we focus on the zero-forcing beamforming technique for MU-MIMO.

### 2.2 MU-MIMO Performance Limitations

The key to the success of this precoding operation is that  $H \cdot W$  is the identity matrix so the transmitted streams are received separately at each receiver. We focus on two characteristics of  $H$  that can degrade the performance of this precoding operation: an ill-conditioned  $H$  [35] or an out-dated  $H$  [23].

An ill-conditioned  $H$  matrix renders matrix inversion inaccurate [18] and thus  $H \cdot W$  is far less likely to equal  $I$ . This results in inter-stream interference degrading the received signal strength of a data stream to its intended receiver [23]. Ill-conditioned  $H$  matrices are a result of receiver channel correlation, an environment and frequency dependent characteristic that will be discussed in § 4.1.

Out-dated  $H$  matrices are a direct result of the latency between the measurement of the  $H$  matrix and the transmission of the  $W$  precoded data streams. Increased time between the measurement of  $H$  and the transmission of  $W \cdot \text{Tx}$ , results in a higher probability of incorrect transmit precoding. Essentially, the transmitter measures  $H_t$  and then calculates  $W_t = H_t^\dagger$ . However, the subsequent precoded transmission is  $H_{t+\Delta} \cdot W_t$ , which may not equal



In order to verify the correctness of the implemented design and understand how manufacturing process variation might effect the output frequency response of multiple RF chains in a MU-MIMO system, we built a Python-based batch interface to the WURC’s serial UART in order to sweep transmit frequencies while simultaneously controlling a bench-top vector signal analyzer to measure the output power. We implemented a digital frequency synthesizer within the digital baseband reference design in order to generate a constant-power complex sinusoid for ease of measurement.

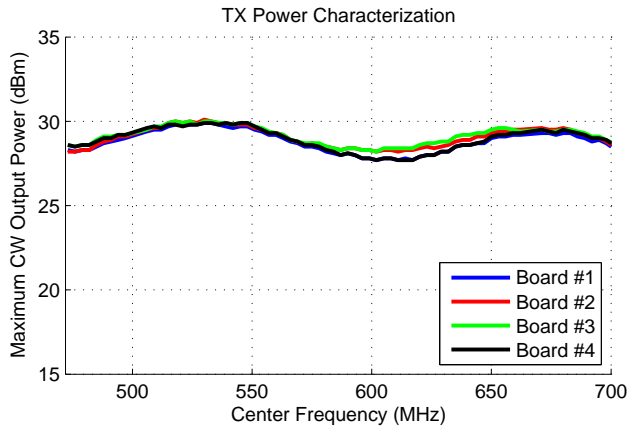


**Figure 3: Process variation across multiple fabricated WURC boards has a small effect on output power.**

The process variation plot in Fig. 3 was generated by increasing the output transmit gain of each WURC at each center frequency until its output PA began to saturate. This is the delivered output power of WURC near the 1dB compression point of the RF chain. Notably, the process variation across different boards is less than 1 dB, with passband ripple on the order of 2.5 dB. This means that multiple RF chains will maintain similar output power across the entire UHF frequency range.

### 3.1.3 Radio Architecture

WURC uses a *direct-conversion* quadrature transceiver architecture based around the LMS6002D “field-programmable” transceiver IC in order to minimize size, implementation complexity, and energy-consumption [2]. Because of this, we are able to power the high-power RF chain from the FMC/HSMC-compliant daughtercard slot, further decreasing size and complexity.

All 12-bit DACs/ADCs, programmable analog anti-aliasing channel filters, frequency synthesizers, and direct-conversion mixers are integrated on a single chip while the rest of the board contains power amplifiers and filters, antenna diversity DPDT switch, power distribution, and a microcontroller (Fig. 2). We designed and tested fast-switching control circuits on the discrete amplification stages that allow the system to operate as a TDD transceiver with a switching time of less than  $7 \mu s$ , or an FDD system with independent transmit and receive fractional-N frequency synthesizers.

**Clocking.** Since the transmit and receive chains in a MU-MIMO base station require precise phase synchronization, WURC was designed to draw RF reference clocks from the host digital baseband board as in Fig. 4. We placed an additional RF reference and sampling clock buffer on the FMC/HSMC adaptor rather than on the daughtercard itself so that the designed system can scale up to four WURCs driven from a single host FPGA with synchronized clocks; however, we only implement a single-radio adapter at this time.

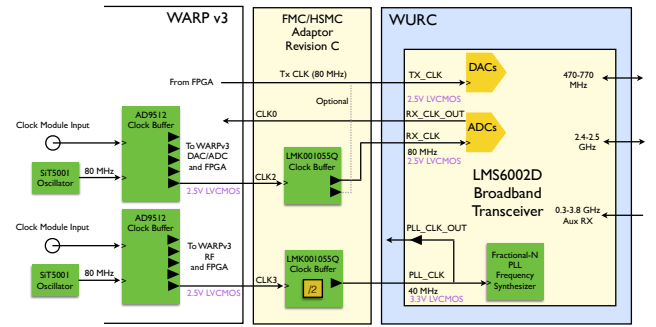


**Figure 4: Source-synchronous sampling clocks and RF reference clocks are buffered in stages, permitting daisy-chaining and future fanout to multiple radios.**

**Control and Calibration.** An on-board micro-controller provides a simple, scriptable, two-wire UART or USB UART interface to a host system for command and control of analog parameters such as center frequency, transmit power, and analog channel bandwidth, while providing full read/write configuration register access to the transceiver.

We designed embedded libraries complete with calibration macros that offload complex computation from the host system and handle the loading of stored factory calibration values for transmit and receive baseband IQ-imbalance and local oscillator feed-through compensation. In addition, we developed automated “factory” calibration procedures that allow us to rapidly calibrate a large number of WURCs for field deployment with minimal setup time.

Each WURC is a highly-integrated SDR front-end module that provides unprecedented capabilities in a small form factor, enabling a wide range of experimental trials and system implementations with excellent RF flexibility.

## 3.2 WURC Array

In order to evaluate MU-MIMO transmissions at various carrier frequencies and node topologies, we integrate WURC and four WARPv3 modules into a coherent 4-radio array.

**Clock Sharing.** The MU-MIMO WURC array combines four WARPv3 boards and 4 WURC daughtercards into a single prototype base station providing combined sample and RF-reference clock synchronization, power, and structural support. Synchronization of reference clocks for ADC sampling and RF frequency synthesizers is required for coherent beamforming and is accomplished by forwarding a daisy-chained reference clock from one master WARPv3 baseband board to the others in the array. All radios derive their sampling and RF reference clocks from this forwarded clock and thus remain phase-synchronized.

**Antennas.** Most studies of UHF propagation involve large, directional antennas intended for signal reception over many kilometers. This is because optimal signal reception and transmission requires antennas of at least  $1/2$  wavelength to generate a resonating standing wave. On the other hand, a Wireless LAN (WLAN) deployment utilizing UHF frequencies may wish to keep the size of the base station somewhat limited, particularly for indoor deployments. For our experiments, we utilize off-the-shelf passive, omnidirectional 3 dBi DTV antennas (August DTA240) that would provide the largest range of coverage with minimal dependance on direction. In our experimental platform (Fig. 5), it is actually the dual-band 2.4/5.8 GHz band antennas (L-com HG2458-5RD-RSP with 3 dBi and 5 dBi gain, respectively) that are larger in size.

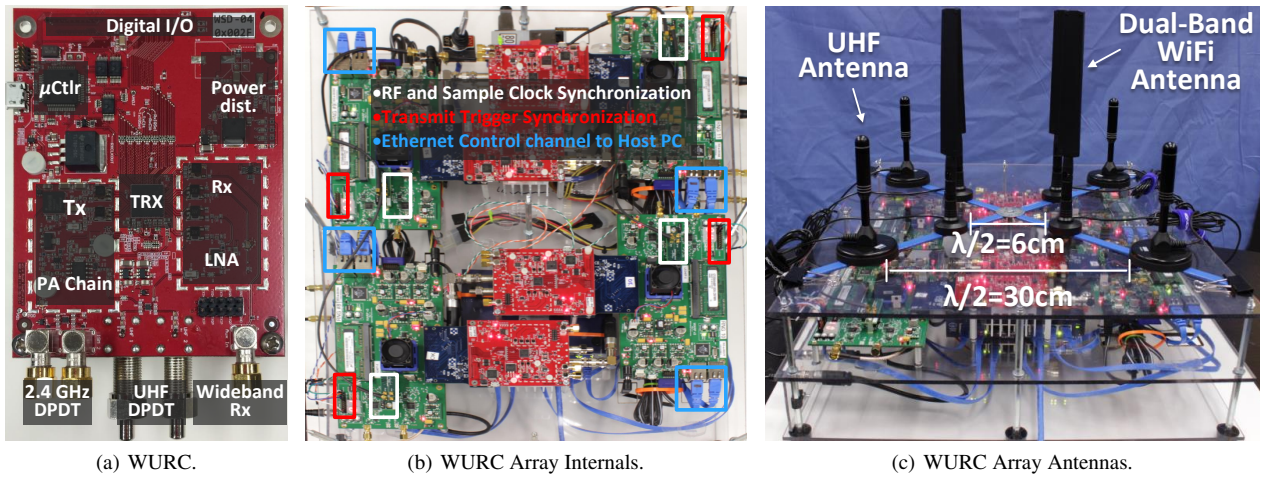


Figure 5: Wideband UHF Radio Card (WURC) hardware platform.

This type of omni-directional antenna array is ideal for indoor MU-MIMO as it provides many opportunities for multipath reflections [9]. In order to guarantee the required channel diversity, each antenna was spaced at least  $1/2$  wavelength for its respective transmit frequency.

### 3.3 Software Framework

In addition to the development of custom hardware to meet our design requirements, we build upon or modify a number of existing applications in order to develop an experimental framework for the WURC MU-MIMO array.

#### 3.3.1 WARPLab

The WARPLab 7 framework for WARP hardware provides a means to pre-compute baseband signals in MATLAB, load transmit sample buffers into an array of WARP boards, and then trigger a simultaneous RF transmission of all buffered signals via a back-end ethernet network or a GPIO trigger [6]. Similarly, an arbitrary number of radios can be configured to perform automatic gain control (AGC) and store their received RF samples in buffers for off-line retrieval and processing.

We extend WARPLab’s object-oriented framework with additional classes and methods to support the WURC’s interfaces. This system provides a powerful workflow for UHF PHY prototyping and measurement studies for multi-antenna systems.

**Measurement Speed.** WARPLab 7 contains a number of transport improvements that result in the ability to perform near-real-time experiments by rapidly performing cycles of: precompute, load, transmit/receive, fetch, and process on the order of 2.5 ms. A fast central coordinator using jumbo ethernet frames for transporting IQ buffers and a compiled MATLAB-mex transport layer can operate at per-packet time intervals. We observed that extra switches between WARPLab nodes produce measurable switching delay and recommend the use of long ethernet cables and minimization of the number of ethernet hops for backhaul.

While powerful, the primary drawbacks of WARPLab is that it requires a central coordinator connected via gigabit ethernet switches, and real-time protocol implementations generally require processing at sub-packet timescales. These two factors hinder long-distance or mobile experiments.

**SINR Measurement Technique.** In order to overcome these limitations yet still accurately measure the MU-MIMO channel, we

employ a WARPLab-based MU-MIMO transmission framework that is based on measuring received SINR and then computing the Shannon capacity to estimate the achievable rate of a transmission system. This is accomplished by a measurement technique adapted from [9] and shown in Fig. 6. Here, the transmitter beamforms sections of the transmission packet independently to accurately measure the SINR.

In the depicted  $4 \times 2$  transmission example, the transmitter first sends an LTS preamble for timing synchronization (blue) and then performs a MU-MIMO transmission to both users (red). In the following two sections (green, purple), the transmitter sequentially zeroes out the steering vector to each receiver in order to measure noise and interference at each receiver during a MU-MIMO transmission. In the example  $4 \times 2$  case, this becomes a single-user beamformed transmission, however in the  $4 \times 3$  or  $4 \times 4$  case, two or three receivers would be beamformed to during this measurement.

Thus, the difference between the full MU-MIMO transmission containing both signal, noise, and interference at each receiver (red) and the transmission containing just interference and noise at the zeroed-out receiver (green or purple) is each transmitter’s SINR. From there, we can compute aggregate Shannon Capacity as  $C = \log_2(1 + \text{SINR})$ .

#### 3.3.2 Real-Time 802.11a/g-Like Reference Design

We realize a real-time 802.11a/g-interoperable design utilizing the WARPv3 802.11 Reference Design and WURC to transmit over UHF frequencies, with modifications to provide 10 and 5 MHz channels [3]. We develop custom HDL for the radio interface, AGC, and digital filtering necessary for a real-time broadband system, and integrate the hardware and software design with the WARPv3 802.11 Reference Design. This system implements a real-time layer-2 wireless bridge utilizing an 802.11a/g AP and STA design with a completely open network stack.

In particular, the real-time capabilities of the 802.11 reference design are leveraged to provide fine-grained continuous channel estimates from multiple transmitting antennas in order to directly measure the MU-MIMO channel capacity instantaneously and over a long period of time.

#### 3.3.3 Framework Enhancements

In order to enable long-range MIMO channel sounding by a large number of mobile nodes, we make the following enhancements and

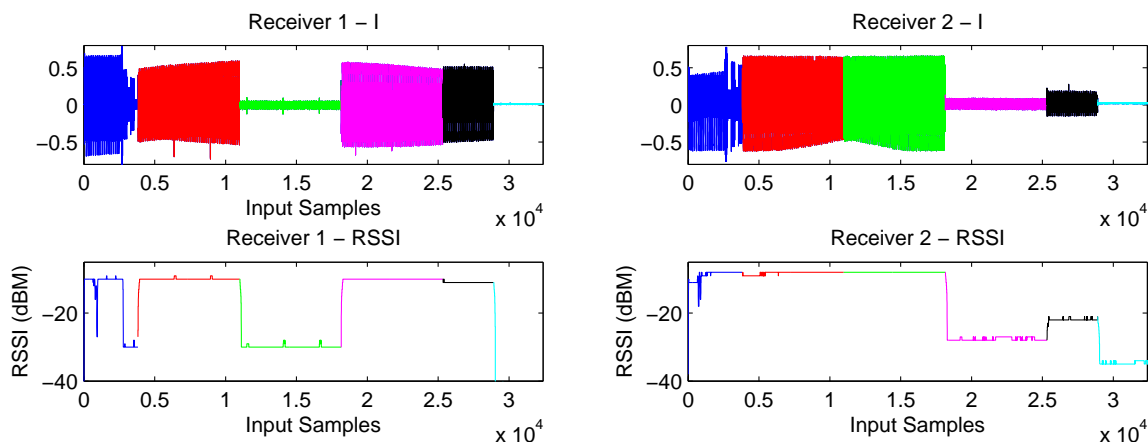


Figure 6: Example RSSI Measurement used in achievable capacity calculation.

modifications to the WARP frameworks described in § 3.3.2 and 3.3.1.

**Hardware Integration.** We adapt both the WARPLab and 802.11 reference design to work seamlessly with the WURC hardware in place of normal WARP daughter cards. From the perspective of the digital baseband, the analog front-end is transparent, which allows interchangeable analog PHYs to be used with the same digital PHY/MAC for fair comparison. This is especially useful for the MU-MIMO comparison study as it controls for a large number of variables in the radio MAC and PHY chain.

**Channel Bandwidth.** The 802.11 reference design operates in a 20 MHz channel bandwidth. In order to enable a UHF transmission to fit within one or two contiguous UHF channels of 6 MHz, we modify the 802.11 reference design to operate at 10 and 5 MHz channel bandwidths in compliance with the 802.11 standard. This is accomplished by halving the data sampling rate with added programmable decimation filters and adjusting MAC parameters and receiver DSP blocks to match.

**Automatic Gain Control.** The range of received power in realistic deployments is sufficiently large that an AGC subsystem is required to guarantee the robust and accurate reception of wide-band channel sounding packets, particular when wireless nodes are mobile. Reference designs from the WARP project rely on external power detectors and autocorrelation to detect incoming packets and estimate a target receive gain setting, whereas an external power detector would require additional external circuitry on WURC.

Instead, we design a custom real-time digital loop in hardware to provide AGC convergence within  $5.6 \mu s$  as required by the 20 MHz 802.11 PLCP and utilizing only the ADC output for packet detection and power estimation. AGC is an enabling technique required to ensure that channel measurement samples have the proper resolution. This is guaranteed when the received signal strength at the ADC input falls within the dynamic range of the ADC (the ADC's ENOB is 10 [2]).

Fig. 7 depicts the performance of the implemented power estimator and AGC subsystem design by reporting a series of experiments over a cable between two WURC nodes with a variable attenuator. The transmit gain is fixed to 25 dB and a 802.11g-like packet with random data payload and 16-QAM OFDM modulation is constructed in MATLAB and transmitted over the cable using the WARPLab framework developed in § 3.3.1. The received packet without Forward Error Correction (FEC) is decoded and its received EVM is calculated as the mean across subcarriers and

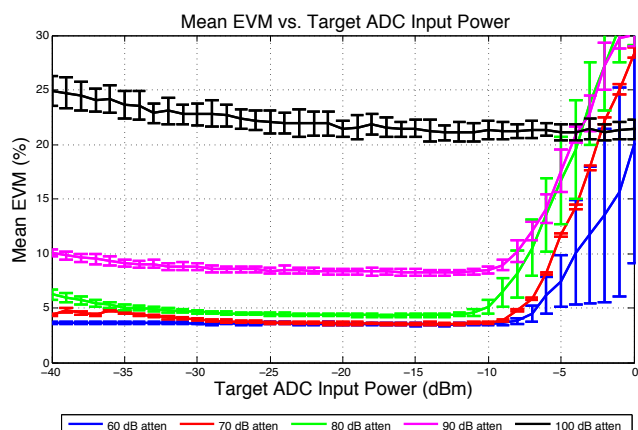


Figure 7: Verification of the implemented received power estimator and AGC operation. Measured with Tx gain at 25 dB, with 16-QAM OFDM modulation.

OFDM symbols of the normalized distance between the received decoded symbol and the intended decoded symbol.

Both the RF path attenuation and target ADC input power are varied under these conditions, resulting in the plot shown in Fig. 7, where the error bars represent one standard deviation across 50 trials. The top plot shows that the ADC operating target of -26 to -13 dBm is optimal for received EVM under a wide range of input powers. For each attenuation value, the bowl of the EVM curve represents the lower bound on the system's 16-QAM receive EVM, with the right-most bound of this range limited by saturation at the ADC and the left-most bound is determined by the system noise floor and quantization error. As expected, high signal attenuation of 100 dB results in a decrease in SINR and thus, minimum achievable EVM. We therefore fix our target ADC input power to -18 dBm in order to ensure that channel measurement packets are detected and received without quantization error and with maximum precision.

**Channel Sounding.** While the legacy 802.11 design calculates and stores channel state information as required by its OFDM channel equalizers, this information is generally discarded after packet reception. The channel estimation extracted from each received 802.11 PLCP header [21] provides a complete CSI estimation matrix that can be used as a single-antenna sounding event. We modify

the physical layer of the 802.11 reference design to treat each of a series of transmitted PLCP headers as separate “packets” for the purpose of CSI measurement from multiple transmitting antennas.

Our custom sounding “packet” is a brief 802.11g-like signal containing PLCP header for packet detection, AGC convergence, and symbol timing extraction. The payload is just long enough to provide error detection bits and identifying information about the transmitter so that the transmitting antenna can be identified. Due to the small size of this sounding packet, it is not compliant with the requirement that 802.11 packets contain an 802.11 and link-layer header. Therefore, we modify the MAC software to pass all packets regardless of valid header or fields to the Ethernet interface for processing.

We construct this special sounding packet in MATLAB and pre-configure the WURC array, running our WARPLab modification, to transmit these packets continuously staggered in time as shown in Figure 8. Tests show that WARPLab continuous-transmit mode remains synchronous over long periods of time if the boards are clock synchronized. We provide sufficient spacing between sounding packets to allow the 802.11 PHY to process the previous packet and reset, and we find that the WARPLab buffer size of 32768 samples over 819.2  $\mu$ s is sufficient to capture channel variation even at higher frequencies.

We combine this structure with a set of multiple listening nodes that process these channel sounding packets and can then store them for later retrieval. A ten-minute packet trace for a single antenna can run over 1 GB in size, so substantial buffering and disk I/O speed is required for the recording nodes.

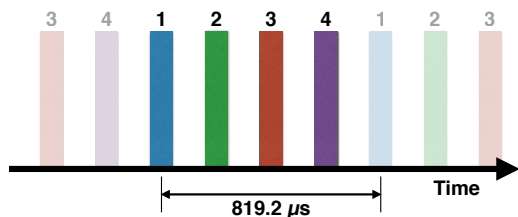


**Figure 8: Short timing packets are sent from each of the WURC array antennas in rapid succession consisting of an 802.11 PLCP preamble and a short, 14-byte payload.**

## 4. MODEL-DRIVEN EVALUATION

In order to understand how different environments and operational frequencies will effect the performance of a MU-MIMO system, we first turn to modern statistical MIMO channel models [24]. Since this statistical model requires tuning for different environments and frequencies, we compare the results using two published parametrizations for 300 MHz [36] and 5.8 GHz [27]. These results provide the theoretical motivation for over-the-air experiments to explore common application scenarios for UHF and 2.4/5.8 GHz WiFi.

### 4.1 UHF vs. 2.4/5 GHz: Channel Models

Spectrum differences between 2.4/5 GHz WiFi and sub-gigahertz frequencies are essentially due to the different manifestations of Doppler effects given each band’s wavelength. Doppler effects are a result of transmitter, receiver, and client movement with respect to a transmission’s wavelength. Because sub-gigahertz wavelengths are 2-4 times longer than 2.4/5 GHz, environmental variation will

affect sub-gigahertz transmissions 2-4 times less (without considering multi-path effects).

Fig. 9 shows the theoretical, freespace 50% coherence time for various sub-gigahertz and 2.4/5 GHz frequencies [28]. The 50% coherence time is expected length of time that the channel characteristics will vary at most 50% given some velocity (effectively channel variation).

The coherence time difference between 2.4/5 GHz WiFi and sub-gigahertz frequencies is between 1-2 *orders of magnitude*. This channel characterization does not consider many real world effects such as multi-path or fading but provides a coarse characterization of the key differences in the two bands.

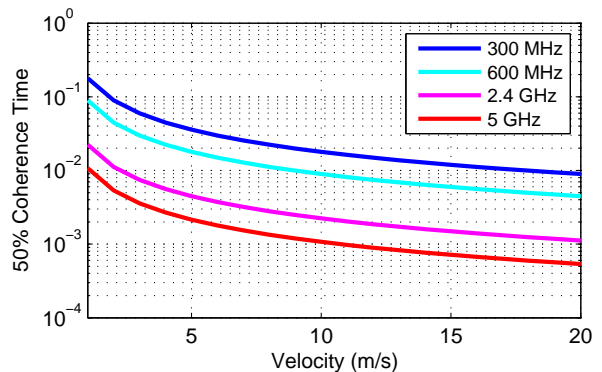


**Figure 9: 50% coherence time for various sub-gigahertz and 2.4/5 GHz WiFi frequencies.**

For a more realistic characterization of the spectrum differences, we employ the COST 2100 MIMO channel model, a flexible channel model that is well suited for MU-MIMO scenarios [24]. This channel model is tuned with parameters that are extracted from empirical measurements and thus does consider real-world channel effects such as fading, multi-path, and non-line-of-sight (NLOS) transmissions. Parametrized realizations of the COST 2100 model have been created for 300 MHz [36] and 5 GHz [27] bands. Using these models, we generate 15,000 channel snapshots at a simulated rate of 100 snapshots per second to characterize the variation of channel state over time and the separability of individual users. Specifically we explore the temporal correlation and receiver separability (shown in Fig. 10) of the generated matrices.

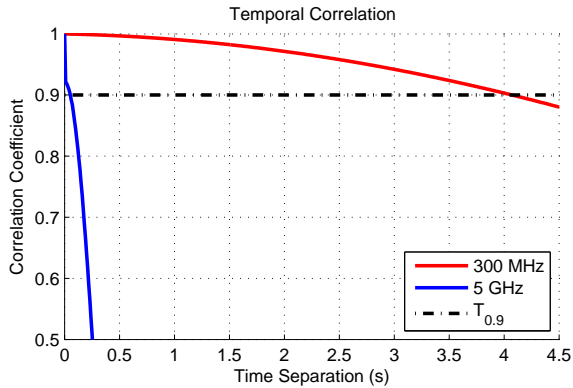
Temporal correlation is the average autocorrelation between channel snapshots at varying intervals of time calculated as described in [31]. The correlation coefficient at time  $\rho$  at time interval  $\ell$  is defined as:

$$\rho_\ell = \frac{\mathbb{E}[H_{mn}[k]H_{mn}^*[k + \ell]]}{\mathbb{E}[H_{mn}[k]H_{mn}^*[k]]} \quad (3)$$

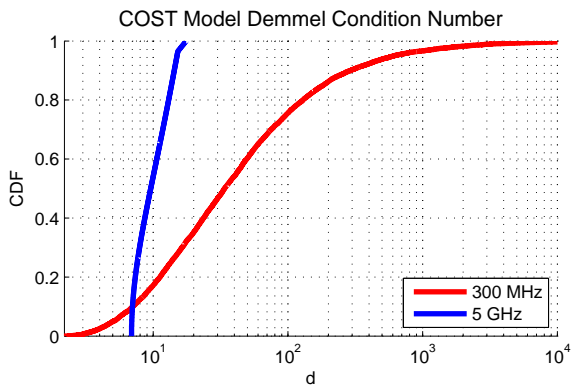
where expectation is calculated for all combinations of transmit antenna  $m$ , receive antenna  $n$  and starting time sample  $k$ .

We show the magnitude of the temporal correlation coefficient in Fig. 10(a) for our generated channels. Lower temporal correlation results in less robust MU-MIMO transmissions because the measured channel state has a high probability of being stale. As seen in Fig. 10(a), the temporal correlation of 5 GHz WiFi almost immediately drops to below 0.9 ( $T_{0.9}$ ) a point when when re-sounding the channel is strongly suggested [11].

According to the channel models, the approximate re-sounding time for 5 GHz is 50 ms and 300 MHz is approximately 4.5 s (almost two orders of magnitude longer). This result is similar to what



(a) Temporal correlation between channel snapshots from 0 to 10 seconds apart. Higher time correlation allows for more robust MU-MIMO performance.  $T_{0.9}$  is 50 ms and 4 s for 5 GHz and 300 MHz respectively.



(b) CDF of model-generated Demmel condition number. Left is better for MU-MIMO

**Figure 10: Temporal correlation and channel condition of 300 MHz and 5 GHz 2x2 MU-MIMO channels generated by COST 2100 MIMO channel model.**

we expect from Doppler effects of the different frequency bands (Fig. 9) and is similar to our indoor temporal characterization in § 5.1.

User separability refers to how well a multi-antenna transmitter can serve a set of users in parallel. The Demmel condition number is a modified matrix condition number that directly predicts the efficacy of an adaptive MIMO or MU-MIMO transmission for a particular channel realization [35].

The Demmel condition number is computed using the eigenvalues  $\lambda_k$  of  $HH^\dagger$  as:

$$d \triangleq \frac{\sum_{k=1}^n \lambda_k}{\lambda_n} \quad (4)$$

where  $\lambda_1 > \lambda_2 > \dots > \lambda_n$ . This ratio represents how well a matrix can be inverted, a key component of many adaptive MU-MIMO techniques such as Zero-Forcing Beamforming [34] and MMSE [30]. Specifically, the higher the condition number, the more numerically unstable the inverse and thus the more inter-user interference during MU-MIMO transmissions reducing received SINR. The condition number ranges from 1 to infinity for well to ill-conditioned matrices, respectively.

This method of calculating the condition number is less forgiving than the traditional singular value ratio. The singular values of

$H$  are the square root of the eigenvalues of  $HH^\dagger$ . Thus, instead of  $\sigma_k/\sigma_n$ , the Demmel condition number is equivalent to  $\sum \sigma^2/\sigma_n^2$  meaning that channel matrices with low singular values (resulting in inaccurate inversion) are even further “penalized.” This modification to the condition number better predicts MU-MIMO performance, in fact, it is consistent and accurate enough to be used for determining parameters such as supported modulation rate and user selection [35].

The COST channel models show a significant difference between the 5 GHz WiFi and UHF bands. The CDF shown in Fig. 10(b) depicts how almost all of the generated 5 GHz channel matrices have a Demmel condition number less than 10 while UHF’s channel condition varies far more and is significantly worse. This results in an increased ability for a MU-MIMO transmitter to invert the channel matrix and send orthogonal streams to each intended user.

Thus, existing MIMO channel models show that while the UHF channel is more temporally stable over time, its ill-conditioned channel matrices can result in lower served SINR due to inter-user interference. However, the available parametrizations of the COST model are for indoor 5 GHz and outdoor UHF scenarios. We show in § 5 how restricting these bands to these transmission environments does not tell the full story.

## 5. EXPERIMENT-DRIVEN EVALUATION

The models analyzed in § 4 are parametrized for particular environments, frequency bands, and topologies. While they suggest that the performance of MU-MIMO beamforming in UHF bands may be advantageous, it is difficult to directly predict or simulate UHF performance using these models as they were not validated for application scenarios such as indoor or urban outdoor, nor the UHF frequency band.

In order to address uncertainty in these models for our target application (indoor and outdoor WLAN), we perform a set of experiments utilizing our custom SDR radio platform that allows us to measure the performance of a MU-MIMO transmission over a diverse set of carrier frequencies and characterize the wireless MU-MIMO channel for important temporal and spatial correlation properties.

We perform over-the-air beam-forming transmissions in a densely packed, challenging office scenario with multiple subscriber nodes and demonstrate not only the ability to simultaneously beamform to distinct users in relatively close proximity, but also the relative improvement that shifting to UHF frequencies provides.

Finally, we perform two sets of experiments with a customized MAC and PHY designed to gather dense, wideband, over-the-air channel estimates in realistic indoor and outdoor WLAN scenarios with multiple subscriber nodes. Using this data, we then demonstrate that the spatial correlation for outdoor users remains similar to that of 2.4 GHz WiFi, thus incurring no beamforming “penalty” for utilizing a frequency band with superior propagation and temporal correlation.

### 5.1 Indoor MU-MIMO Transmissions

**Experimental Setup.** First, we evaluate the performance of UHF MU-MIMO in an indoor, NLOS, office environment. Experiments were conducted during the work day with people walking through the halls in the environment depicted in Fig. 12.

The transmitting array was placed on a third floor walkway bridge and 6 separate receivers in two adjacent offices within the adjoining hallway. Note that the to-scale depiction in Fig. 12 shows the relative co-location of all receiving nodes with respect to the distance from the transmitter to simulate a densely packed

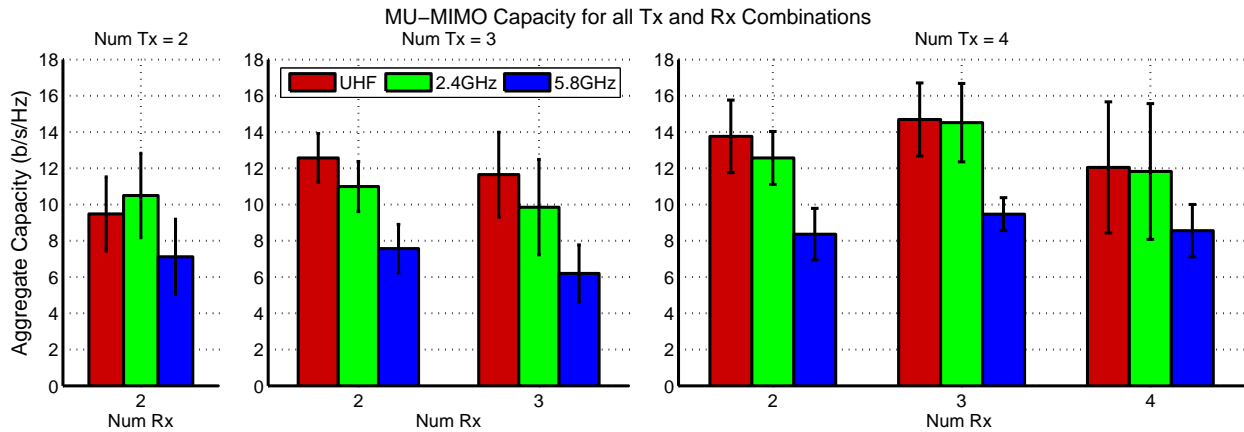


Figure 11: Received MU-MIMO Capacity.

office environment. This represents a realistic, challenging case for indoor stationary MU-MIMO transmissions due to the co-located receivers.

To encompass a wide range of user grouping conditions, every possible combination of transmit and receive antennas are considered. Sixty transmissions are performed for each topology. The center frequencies for each frequency band (*i.e.* channel) were chosen so that transmissions did not encounter interference from other equipment. Specifically, the UHF channel was first directly scanned for existing DTV or microphone transmissions and an experimental license was obtained to operate equipment on that channel. The channels selected for 2.4 and 5.8 GHz are not currently supported by the regulatory domain where these experiments were performed, thus ensuring minimal ISM-band interference. Using the measurement technique specified in § 3.3.1, every possible topology’s MU-MIMO capacity is measured for each frequency band and shown in Fig. 11.

**MU-MIMO Achievable Sum-Rate Capacity.** Based on the channel models and accompanying analysis presented in § 4.1, we expect that the increased spatial correlation of UHF channels will not allow for MU-MIMO transmissions to accurately separate nearby users. However, we find that UHF MU-MIMO transmis-

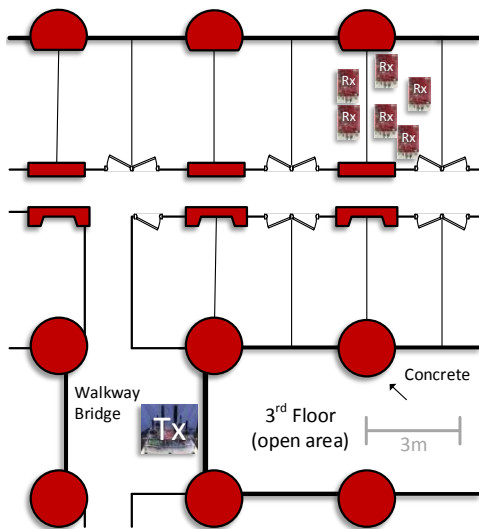


Figure 12: Indoor Experimental Test Setup.

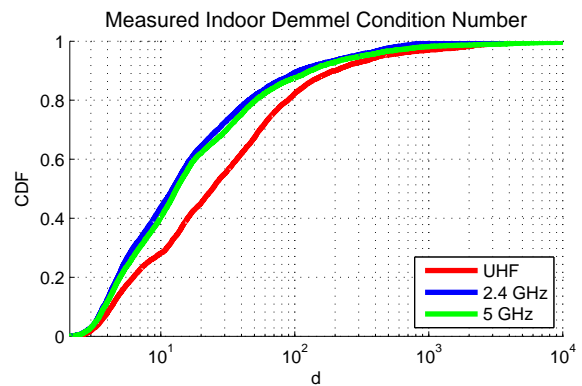


Figure 13: Demmel condition number measured for the indoor environment. Left is better for MU-MIMO.

sions can actually achieve a sum capacity similar to that of 2.4 GHz WiFi transmissions (always between 1-2 b/s/Hz above of below the 2.4 GHz band).

In fact, we find that majority of the intuition and channel models surrounding UHF MU-MIMO are not specific to the frequency band itself but rather generalized characteristics of MU-MIMO transmissions. For example, the available MU-MIMO channel models characterize *indoor* WiFi and *outdoor* UHF channel environments where, regardless of frequency band, we expect increased difficulty in user separability in outdoor environments. Note the channel condition of the different transmission bands in the NLOS environment in Fig. 13 are similar in contrast to Fig. 10(b). Even though the wavelength of UHF is longer resulting in better propagation through materials, the UHF-band transmission still experiences enough multi-path to successfully beamform to multiple users in parallel.

Additionally, the results shown in Fig. 11 show a known trend of achievable capacity for MU-MIMO transmissions where the MU-MIMO gain plateaus as the available Degrees of Freedom (DoF)<sup>1</sup> are reached. The consistently worse performance of 5.8 GHz is explained by the high attenuation experienced by that frequency band in NLOS conditions combined with its sensitivity to environmental variation.

<sup>1</sup>DoF here refers to how many more transmit antennas there are than receive antennas in a MIMO transmission.

Note that UHF MU-MIMO consistently outperforms 2.4 GHz transmissions except for in the 2x2 transmission scenario. Because the sum transmit power emanating from the array is held constant regardless of the number of transmit antennas in use, the performance differential is solely a result of channel state, specifically it is an indicator of temporal channel correlation due to the WARPLab measurement platform.

As discussed on § 3.3.1, the latency in the WARPLab platform is due to the rate at which the host PC can download and upload samples to each of the WARP boards over Ethernet. In our system, we benchmark a read/write rate of approximately 2.5 ms per buffer and the closed loop beamforming method employed requires between 10 to 20 ms to complete depending on the number of transmit and receive antennas (the difference between a 2x2 and 4x4 transmission scenario).

**Measured Temporal Correlation.** To gain additional insight into the measured capacity results and to infer real world performance from our MU-MIMO transmissions, we also consider the channel correlation measured during each experiment.

For each topology, we consider each of the 60 MU-MIMO transmissions and their channel matrices. We calculate channel correlation between varying times during the experiment to measure the rate of change of the channel information with respect to time. These calculations are an average over all topologies (all combinations of transmit and receive antennas).

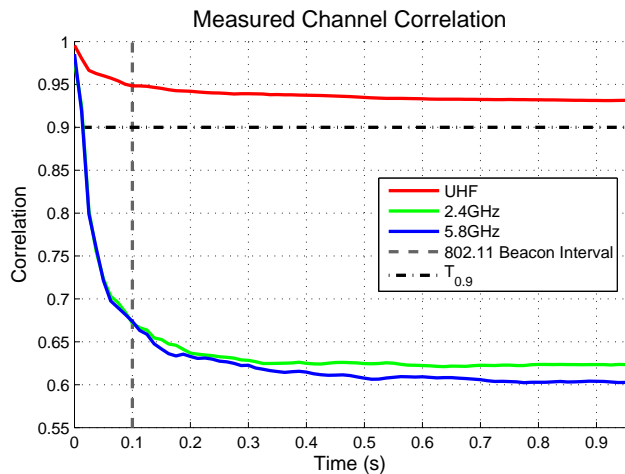


**Figure 14: Measured Temporal Channel Correlation, depicting Beacon Interval, and  $T_{0.9}$ . WARPLab latency is 10-20 ms depending number of transmit and receive antennas.**

Fig. 14 shows how the channels decorrelate over the course of one measured second in time. This is effectively an indicator of how long a transmitter has after measuring the channel matrix and before actually transmitting parallel streams using that measurement. A coherence time of  $T_{0.9}$  represents when the probability of the channel being too stale to successfully beamform over is high.

First, note that the WARPLab latency range of 10 to 20 ms is approximately  $T_{0.9}$  for the the two WiFi frequency bands. This indicates why only the 2x2 transmission scenario has the 2.4 GHz transmitter outperform UHF MU-MIMO; the latency between the sounding and transmission phase was the lowest and just at the  $T_{0.9}$  limit.

While the 2.4/5 GHz frequencies both drop significantly within 100 ms, UHF remains above the  $T_{0.9}$  threshold for the maximum one measured second difference between channel matrices. While

these correlation values are not asymptotic and will eventually degrade, the performance of 2.4 and 5.8 GHz is sufficiently low for stationary devices [11].

Also note that the 802.11 beacon packet rate (100 ms) is greater than the interval that 2.4/5 GHz MU-MIMO channels decorrelate. However, the stability of the UHF channel implies that a UHF MU-MIMO system could use periodic protocol packets for exchanging channel state information.

Finally, the channel correlation result shown in Fig. 14 effectively scales the MU-MIMO achievable rate shown in Fig. 12. The rate at which the 2.4/5 GHz channel decorrelates necessitates channel sounding on a per packet basis adding considerable overhead to MU-MIMO transmissions. However, the temporal stability of the UHF MU-MIMO channel allows a transmitter to significantly reduce this overhead intensive sounding process and thus significantly increase the potential MU-MIMO gains.

## 5.2 Outdoor Channel Characterization

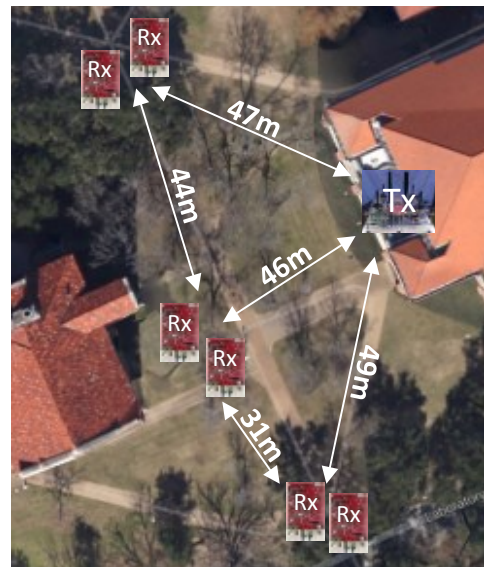


**Figure 15: Experimental setup for outdoor channel sounding experiments. Distances between transmitter (on third floor balcony) and receivers shown. Note building and tree locations.**

Finally, using the experimental framework developed in § 3, we perform outdoor channel sounding experiments to directly compare the performance and stability of UHF MU-MIMO channels. To that end, we setup an experimental network of a collection of nodes located outdoors being served by our array from a third floor balcony. Although the UHF transmitter is capable of transmitting much further distances, we limited the scale of the topology as shown in Fig. 15 to ensure a fair comparison between UHF and 2.4/5 GHz bands. The locations of the nodes were chosen such that the transmissions from the UHF and 2.4/5 GHz bands would reach the receivers (the UHF band transmitters can easily transmit further than 50 m). However, even by reducing the receiver distance to what is shown in Fig. 15, the 5 GHz band transmissions did not reliably reach the receiving nodes severely limiting the number of measured channel matrices. Thus, we restrict our outdoor comparison to the UHF and 2.4 GHz bands.

Just as we evaluated temporal correlation in the multi-path rich, indoor transmission environment, we seek to similarly characterize the most detrimental aspect of the outdoor MU-MIMO channel: re-

ceiver separability. Ill-conditioned channel matrices, as discussed in § 4.1, have a detrimental effect on an MU-MIMO enabled transmitter’s ability to separate multiple users.

In the previous section, we found that while temporal stability of UHF was greater than that of 2.4/5 GHz, spatial correlation did not suffer as the UHF MU-MIMO transmissions were able to separate the co-located receivers. However, in an open, outdoor line-of-sight (LOS) environment, we find that both the UHF and 2.4 GHz bands exhibit the same Demmel condition number. Additionally, the CDF of the Demmel condition number closely matches the COST UHF channel condition shown in Fig. 10(b). This suggests that the comparison shown in Fig. 10(b) is not a result of the frequency band itself, but rather the wholly different channel environments in which the model was parametrized.

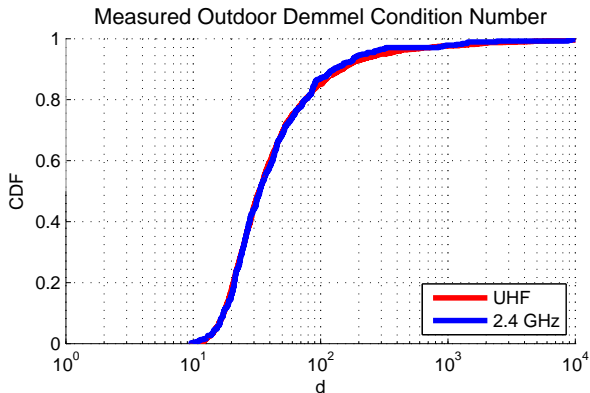


Figure 16: Measured Demmel Condition Number of the outdoor MU-MIMO channel.

## 6. RELATED WORK

We separate the discussion of related work into platforms and testbeds and UHF band characterization.

### 6.1 SDR Platforms

A number of common development platforms are capable of some degree of frequency-agility and programmability, e.g., [1, 4, 5]. However, these platforms are generally limited to either narrow-bandwidth applications when used for real-time applications or lack the open hardware and software stack required for research. None of them contain high-power amplifiers for long-range experiments. The form-factor currently required for real-time operation of platforms performing DSP operations on a CPU [1, 4] becomes a limitation when measuring wideband channel statistics for long periods of time with high temporal granularity, as such experiments often require many mobile user nodes.

Furthermore, existing systems do not integrate all components (specifically, a high-power analog front-end or highly dynamic AGC subsystem) necessary for high-bandwidth, long-range experiments. Off-the-shelf UHF amplifiers often are not designed for frequency-flat, wideband operation between 470-698 MHz and their size and external power requirements further hinder the mobility of multiple radio nodes.

WURC is designed to work interchangeably with any digital baseband and only draws power from the expansion card slot available on most FPGA development boards while integrating the remaining components necessary for a high-powered wideband transceiver. In combination with WURC, the WARP digital baseband platform contains a complete real-time layer 2 network stack and large experimental log storage capabilities (2 GB DDR3 RAM)

within a small form-factor board, making it feasible to build and deploy a large number of wireless, mobile nodes for UHF MU-MIMO experiments.

### 6.2 UHF Band Characterization

**MU-MIMO 2.4/5 GHz Characterization.** While previous work emphasizes the importance of channel coherence time for MU-MIMO systems [9] and theoretical results suggest that center frequency is directly related to channel coherence time [28], these works do not provide the information necessary to perform a comparison based on center frequency. Such an investigation is necessary as MU-MIMO theoretical models for UHF and 2.4/5 GHz WiFi bands are parametrized for different environments (outdoor and indoor respectively). Models suggest that UHF band MU-MIMO exhibits increased temporal correlation at the cost of *increased* spatial correlation compared to 2.4/5 GHz WiFi (which would be detrimental to MU-MIMO due to the difficulty in providing orthogonal streams to the user [9]). However, we show that this tradeoff is not a result of the frequency band; instead, it is a result of the transmission environment. Thus, this discrepancy is not an inherent flaw to existing MU-MIMO channel models; rather, it is a result of incomplete parametrization and comparison of the MU-MIMO channel for all band/environment combinations.

**SISO UHF Characterization.** Several works explore the propagation characteristics of UHF transmissions in a variety of environments and topologies, e.g., [13, 20, 26, 33]. These works exhaustively analyze the performance of packetized UHF transmissions through different materials and in various environments. However, they focus on single-antenna, single-user transmissions and thus the characterization is restricted to metrics such as path loss, delay profile, and attenuation through materials. In contrast, our work focuses on the aggregate effects of these metrics with respect to MU-MIMO transmissions, namely temporal and spatial correlation in outdoor and indoor environments. Additionally, our work focuses on comparing these characteristics to 2.4/5 GHz bands where MU-MIMO techniques are used prevalently.

**MIMO UHF Characterization.** Other works exhaustively characterize MIMO transmissions in the UHF band [10, 15, 19, 22, 25]. However, they focus on outdoor, Single-user MIMO transmissions and thus focus on point to point transmissions with a single transmitter/receiver pair, each equipped with multiple antennas. While single-user and multi-user MIMO transmissions can have an equivalent number of transmit/receive antenna paths, the co-located receive antennas in the single-user case drastically reduces the variability in the temporal and spatial correlation with respect to environmental factors. Thus, the usage scenario of distinct MU-MIMO user nodes separated by some distance is not represented in the existing work. Instead, our work focuses on *multi-user* MIMO transmissions and specifically characterizes the effects of separated receivers.

Lastly, uplink MU-MIMO channels were studied in the UHF-band in a rural outdoor environment [29]. In contrast, we focus on downlink transmissions, consider both indoor and urban outdoor environments and provide channel characterization and spatial correlation of groups of users. Additionally, we evaluate *both* UHF and 2.4/5 GHz band MU-MIMO performance to comparatively characterize the performance of a UHF-band MU-MIMO system and provide an open-source platform.

## 7. CONCLUSION

We design and implement a wideband UHF SDR front-end with the ability to transmit on a diverse set of frequencies. We then utilize this new hardware capability and design an open MU-MIMO

testbed, which we use to perform over-the-air experiments to empirically demonstrate that the UHF band is advantageous for MU-MIMO technologies.

## 8. ACKNOWLEDGMENTS

The authors would like to thank the following people for their assistance in performing experiments included in this work: Rachel J. Gray (Rice University), Yuqiang Mu (Rice University), and Pablo Salvador (IMDEA Networks Institute). This research was supported by NSF grants CNS-1314822, CNS-1126478, CNS-1012831, and a grant from Cisco Systems, Inc.

## 9. REFERENCES

- [1] Ettus USRP. Available at: <https://www.ettus.com>.
- [2] Lime Microsystems LMS6002D. Available at: <http://www.limemicro.com/products/LMS6002D.php>.
- [3] Mango Communications 802.11 Reference Design. Available at: <http://mangocomm.com/802.11>.
- [4] Microsoft SORA. Available at: <http://research.microsoft.com/en-us/projects/sora/>.
- [5] Nutaq. Available at: <http://nutaq.com/en>.
- [6] Rice University WARP project. Available at: <http://warp.rice.edu>.
- [7] Wurc documentation. Available at: <http://http://www.volowireless.com/products/WURC>.
- [8] Ofcom . Regulatory requirements for white space devices in the UHF TV band, Jul. 2012. Available at: [www.cept.org/Documents/se-43/6161/](http://www.cept.org/Documents/se-43/6161/).
- [9] E. Aryafar, N. Anand, T. Salonidis, and E. Knightly. Design and experimental evaluation of multi-user beamforming in Wireless LANs. In *Proc. ACM MobiCom*, Chicago, IL, Sept. 2010.
- [10] J. Boyer, P. Brown, K. Hayler, M. Garcia, J. Mitchell, P. Moss, and M. Thorp. MIMO for Broadcast—results from a high-power UK trial. In *Proc. IBC*, Amsterdam, The Netherlands, Sept. 2007.
- [11] G. Breit. Coherence Time Measurement for TGac Channel Model. In *IEEE 802.11-09/1173r1*, Nov. 2009.
- [12] Code of Federal Regulations. Title 47, part 15, subpart H - Television Band Devices, Feb. 2009.
- [13] I. Collings, H. Suzuki, and D. Robertson. Ngara broadband access system for rural and regional areas. *Telecommunications Journal of Australia*, 62(1), 2012.
- [14] M. Costa. Writing on dirty paper. *IEEE Transactions on Information Theory*, 29(3):439–441, May 1983.
- [15] G. Eriksson, S. Linder, K. Wiklundh, P. Holm, P. Johansson, F. Tufvesson, and A. Molisch. Urban peer-to-peer MIMO channel measurements and analysis at 300 MHz. In *Proc. IEEE MILCOM*, San Diego, CA, Nov. 2008.
- [16] A. Flores, R. Guerra, E. Knightly, P. Ecclesine, and S. Pandey. IEEE 802.11af: A standard for TV white space spectrum sharing. *IEEE Communications Magazine*, 51(10):92–100, Oct. 2013.
- [17] A. Grebennikov. *RF and Microwave Power Amplifier Design*. McGraw-Hill, 2004.
- [18] A. Greenbaum and T. Chartier. *Numerical Methods: Design, analysis, and computer implementation of algorithms*. Princeton University Press, 2012.
- [19] A. Hammons, J. Hampton, N. Merheb, and M. Cruz. Cooperative MIMO field measurements for military UHF band in low-rise urban environments. In *Proc. IEEE SAM*, Darmstadt, Germany, Jul. 2008.
- [20] J. Hampton, N. Merheb, W. Lain, D. Paunil, R. Shuford, J. Abrahamson, and W. Kasch. Propagation characteristics of ground based urban communications in the military UHF band. In *Proc. IEEE MILCOM*, Atlantic City, NJ, Oct. 2005.
- [21] IEEE P802.11ac/D4.1. Specification framework for TGac, Nov. 2012.
- [22] M. Jung, J.-H. Kim, Y.-K. Yoon, and H.-J. Hong. Multipath characteristics of MIMO channel at the UHF band for wireless systems in the urban area. In *Proc. IEEE ICAC*, Phoenix Park, South Korea, Feb. 2011.
- [23] F. Kaltenberger, D. Gesbert, R. Knopp, and M. Kountouris. Correlation and capacity of measured multi-user MIMO channels. In *Proc. IEEE PIMRC*, Cannes, France, Sept. 2008.
- [24] L. Liu, C. Oestges, J. Poutanen, K. Haneda, P. Vainikainen, F. Quitin, F. Tufvesson, and P. Doncker. The COST 2100 MIMO channel model. *IEEE Wireless Communications Magazine*, 19(6):92–99, Dec. 2012.
- [25] R. Parviainen, J. Ylitalo, J.-P. Nuutinen, P. Talmola, J. Henriksson, H. Himmanen, R. Ekman, and E. Huuhka. Experimental investigations on MIMO radio channel characteristics on UHF band. In *Proc. IEEE ICC*, Dresden, Germany, Jun. 2009.
- [26] V. Pham and J.-Y. Chouinard. A study on the channel and signal cross correlation of UHF DTV channels. In *Proc. IEEE ISSSE*, Montreal, Canada, Jul. 2007.
- [27] J. Poutanen, K. Haneda, L. Lingfeng, C. Oestges, F. Tufvesson, and P. Vainikainen. Parameterization of the COST 2100 MIMO channel model in indoor scenarios. In *Proc. EurAAP EuCAP*, Rome, Italy, Apr. 2011.
- [28] T. Rappaport. *Wireless Communications: Principles and Practice*. Prentice Hall, 2001.
- [29] H. Suzuki, D. Robertson, N. Ratnayake, and K. Ziri-Castro. Prediction and measurement of multiuser MIMO-OFDM channel in rural Australia. In *Proc. IEEE VTC*, Yokohama, Japan, May 2012.
- [30] D. Tse and P. Viswanath. *Fundamentals of wireless communication*. Cambridge University Press, 2005.
- [31] J. Wallace, M. Jensen, L. Swindlehurst, and B. Jeffs. Experimental characterization of the MIMO wireless channel: Data acquisition and analysis. *IEEE Transactions on Wireless Communications*, 2(2):335–343, Mar. 2003.
- [32] B. Yarman. *Design of ultra wideband power transfer networks*. John Wiley & Sons, 2010.
- [33] X. Ying, J. Zhang, L. Yan, G. Zhang, M. Chen, and R. Chandra. Exploring indoor white spaces in metropolises. In *Proc. ACM MobiCom*, Miami, FL, Sept. 2013.
- [34] T. Yoo and A. Goldsmith. On the optimality of multiantenna broadcast scheduling using zero-forcing beamforming. *IEEE Journal on Selected Areas in Communications*, 24(3):528–541, Mar. 2006.
- [35] C. Zhong, M. McKay, T. Ratnarajah, and K. Wong. Distribution of the Demmel condition number of Wishart matrices. *IEEE Transactions on Communications*, 59(5):1309–1320, May 2011.
- [36] M. Zhu, G. Eriksson, and F. Tufvesson. The COST 2100 channel model: Parametrization and validation based on outdoor MIMO measurements at 300 MHz. *IEEE Transactions on Wireless Communications*, 12(2):888–897, Feb. 2013.